Ministry of Education and Science of Ukraine

ODESA NATIONAL UNIVERSITY OF TECHNOLOGY

International Competition of Student Scientific Works

BLACK SEA SCIENCE 2023

PROCEEDINGS

ODESA, ONUT 2023

Ministry of Education and Science of Ukraine

Odesa National University of Technology

International Competition of Student Scientific Works

BLACK SEA SCIENCE 2023

Proceedings

Odesa, ONUT
2023

DEVELOPMENT OF A PLANT FOR THE MANUFACTURE OF WEAR-RESISTANT PARTS OF MINING EQUIPMENT

Authors: Fihol Artem, Dorozhynskyi Serhii
Advisor: Vakhonina Larysa
Mykolayiv National Agrarian University (Ukraine)

Abstract. *Increasing the service life of rural-urban parts. machines is one of the main tasks facing the engineers of the agro-industrial complex. One of the ways to solve this problem is to develop new alloys and improve existing ones. There are many methods of improving the quality of cast metal. Functional capabilities of these methods are multifaceted and multipurpose. But there is no single universal method capable of affecting metal equally effectively. One of these new methods is the treatment of crystallizing liquid metal with an electric pulse discharge. Previous studies have shown that such processing has a sufficiently high efficiency. At the same time, it remains innovative and currently underexplored.*

Therefore, to solve this problem, it is advisable to develop electrical equipment for the implementation of the technology of non-baking processing of metals and alloys.

Keywords: *electrode system, VEO, pulse current generator, pulse, macrostructure of ingots, crystallization process.*

I. INTRODUCTION

Increasing the service life of rural-urban parts. machines is one of the main tasks facing the engineers of the agro-industrial complex. One of the ways to solve this problem is to develop new alloys and improve existing ones. There are many methods of improving the quality of cast metal. Functional capabilities of these methods are multifaceted and multipurpose. But there is no single universal method capable of affecting metal equally effectively. The current state of this issue is developing both in the direction of improving each traditional method and in the direction of finding alternative technological methods of processing. One of these new methods is the treatment of crystallizing liquid metal with electropulse discharge. Previous studies have shown that such treatment has a sufficiently high efficiency.

The purpose of this study is to design an electric discharge unit for out-of-furnace metal processing for the production of wear-resistant parts of agricultural machinery.

In order to achieve the given task, the current state of non-furnace current processing of metals and alloys in the melt and at the crystallization stage was analyzed, simulations of the electric discharge processes of processing metals and alloys with high-voltage pulsed current at the crystallization stage were carried out, electrical engineering equipment was developed for the implementation of the technology of non-furnace processing of metals and alloys, on stages of crystallization, and an experimental study of the influence of the parameters of the electric discharge unit on the crystallization process, structure and properties of aluminum alloys was performed.

II. LITERATURE ANALYSIS

The duration of experimental studies of the processes being studied does not allow them to be analyzed in all the variety of varied parameters. A numerical experiment is more effective in this regard. The data obtained in this way allow us to approach the understanding of the mechanisms of electropulse processing of liquid melt, which are directly related to the electromagnetic phenomena that occur in the melt when an electric potential is applied and the passage of a discharge current [1]. Let's consider different options of electrode systems (Fig. 1), which are most likely to be used in practice:

1) point - plane;
2) point - point;
3) the tip - the walls of the ladle [2].

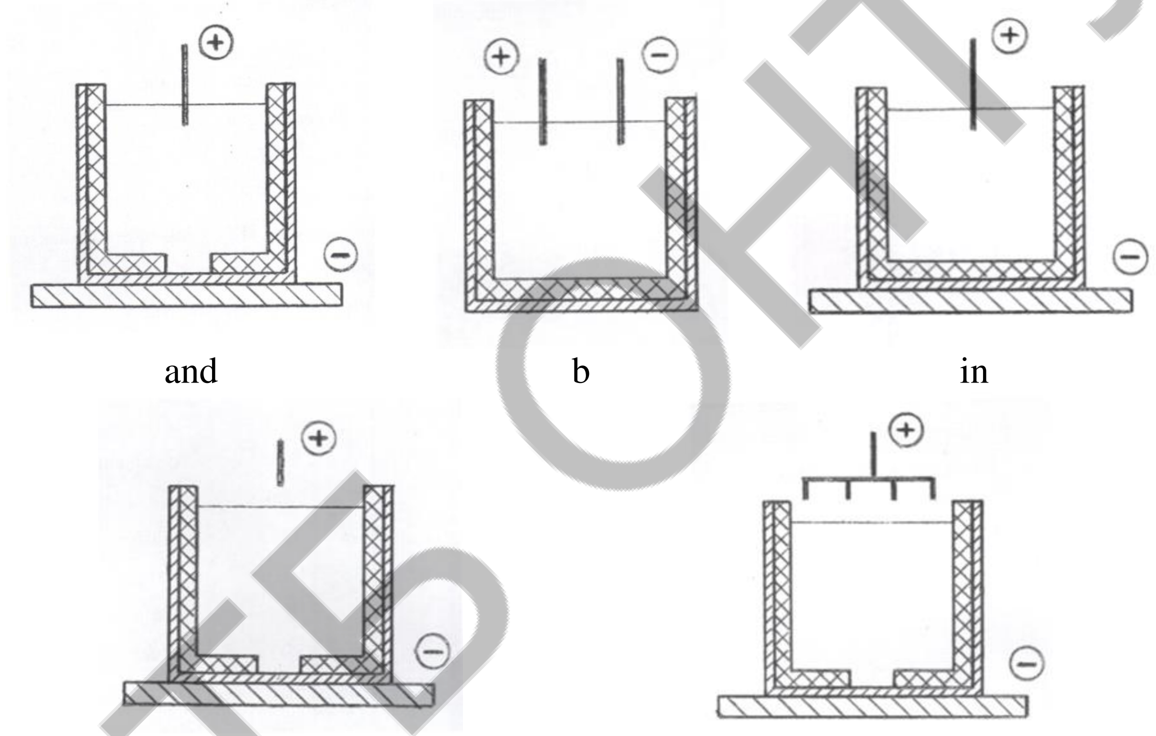

and b in

Mr d

Fig. 1 – Electrode systems for experimental research: a, b, c – for processing the crystallizing melt; a, d, d – for liquid metal processing

Modeling of electromagnetic processes in liquid metal with a macroscopic approach is performed by solving Maxwell's equations with certain boundary conditions. It is appropriate to use the system of Maxwell's equations, written in differential form, because it allows us to use numerical finite-difference methods for solving [3].

In the general case, for quasi-stationary fields, this system of equations is written as follows:

$$\nabla \times H = J = \sigma(E + v \times B) + J^e , \quad (1)$$

$$\nabla \times E = -\frac{\partial B}{\partial t} , \quad (2)$$

$$\nabla \times B = 0, \quad (3)$$

$$\nabla \times D = 0, \quad (4)$$

$$\nabla \times J = 0, \quad (5)$$

where ∇– the Nabla operator; H – magnetic field strength in the melt, A/m; *J*– current density, A/m2; σ – specific electrical conductivity, S/m; *E*– electric field strength, A/m; v – speed of the object, m/s;v=0 B– magnetic field induction in the melt, Tl; – density of induced (extraneous) currents, A/m2; D – electric induction, Kl/m.J^e

We invert the conductivity tensor. Then equation (1) can be written in the form:

$$E = \sigma^{-1}(\nabla \times H - J^e) + v \times B, \quad (6)$$

Let's replace E according to Faraday's law, substituting the most general equation for magnetic induction:

$$B = \mu_0 \mu_r H + B_r, \quad (7)$$

where B_r – induction of external magnetic field, Tl; μ_0 is the magnetic constant, $4\pi \cdot 10^{-7}$ Hn/m; μ_r – relative magnetic permeability, $\mu_r = 1$.

We obtain the general equation for a quasi-stationary electromagnetic field:

$$\frac{\partial}{\partial t}(\mu_0 \mu_r H + B_r) + \nabla \times (\sigma^{-1}(\nabla \times H - J^e) - v \times (\mu_0 \mu_r H + B_r)) = 0, \quad (8)$$

In order to take into account the problems arising in regions with zero conductivity, μ_r and B_r let's represent it as a function of the magnetic field strength, taking the partial derivatives with respect to time. We will get:

$$(\mu_0 H \frac{\partial \mu_r}{\partial H} + \mu_0 \mu_r + \frac{\partial B_r}{\partial H})\frac{\partial H}{\partial t} + \nabla \times (\sigma^{-1}(\nabla \times H - J^e) - v \times (\mu_0 \mu_r H + B_r)) = 0, \quad (9)$$

To solve this equation, we will use the Femlab software environment (system), in particular, its module Quasi-staticfields/MeridionalCurrents/Transientanalys, which allows analyzing processes changing in time by solving differential equations using the finite difference method.

Since the container with aluminum melt has a cylindrical shape, it is convenient to look for the solution in the cylindrical coordinate system (z, r, φ). Dimensions of the conductor (melt) - radius R0 = 45·10-^{3}m; heightHk = 90·10-^{3}m.

We will carry out the calculations using the following parameters of the discharge circuit (which were used for processing) as an example – U0= 31 kV; L= 1.787 μH; C= 1 μF.

2.1. Electrode system "Point - plane"

The "Point - plane" electrode system corresponds to the case when the melt is in a container with lined (non-conductive) walls, and an unlined steel bottom acts as a counter electrode [4]. The geometric model of the conductor is presented in (Fig. 2).

Let us assume that the Z axis coincides with the bucket axis, the angle φ = 0. The magnetic field in the object depends on the angle φ, and the current and electric field depend on r and Z.

Let's assume that the current from the positive electrode E flows into region 5 on the negative electrode.

Let's write down the equation of the magnetic field in a ladle with melt with respect to the variable H_φ. Since there is no external magnetic field source, then $B_r = 0$.

$$\mu_0 \mu_r \frac{\partial H_\varphi}{\partial t} + \nabla \times (\sigma^{-1} (\nabla \times H_\varphi - J^e) - v \times (\mu_0 \mu_r H_\varphi) = 0 , \qquad (10)$$

where H_φ – intensity of the magnetic field in the object, A/m.

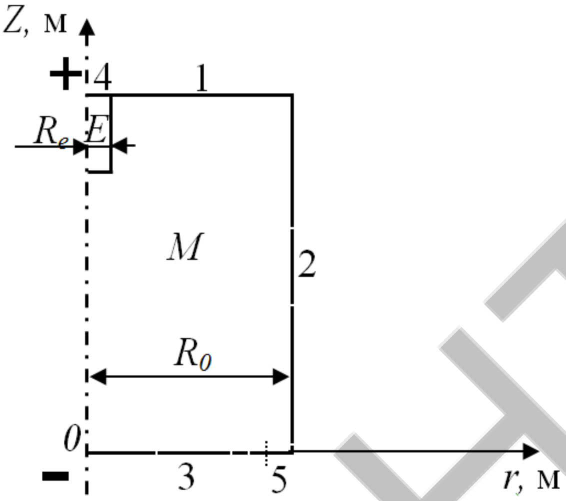

Fig. 2 – Geometry of the conductor for the electrode system "Point - plane"

If equation (10) is solved for the melt, then σ for liquid aluminum is substituted into it. Accordingly, if the electromagnetic field is described inside the electrode, the value σ characterizing solid steel is substituted into equation (10).

Assume that the initial speed of the melt and the density of extraneous currents$v$=0 $J^e = 0$. Suppose that on the axis Z $H_\varphi = 0$ Let's set the initial conditions: $H_\varphi\big|_{t=0} = 0$ and $I\big|_{t=0} = 0$.

Boundary conditions:

For area 1: $$H_\varphi = \frac{I(t)}{2 \cdot \pi \cdot r}, \qquad (11)$$

For area 2: $$H_\varphi = \frac{I(t)}{2 \cdot \pi \cdot R_0}, \qquad (12)$$

For area 3: $$H_\varphi = 0, \qquad (13)$$

For area 4: $$H_\varphi = \frac{I(t) \cdot r}{2 \cdot \pi \cdot R_e^{\,2}}, \qquad (14)$$

For area 5: $$H_\varphi = \frac{I(t) \cdot (r - R_0 + \Delta_{скін})}{2 \cdot \pi \cdot R_0 \cdot \Delta_{скін}}, . \qquad (15)$$

The dependence I(t) can be specified analytically, or, as in our case, numerically, by digitizing the experimentally obtained amplitude-time dependence of the discharge current.

The current lines in this case will be distributed as shown in (Fig. 3), and (Fig. 4) shows the distribution of the amplitude of the magnetic field in different sections of the ladle at the maximum amplitude of the discharge current.

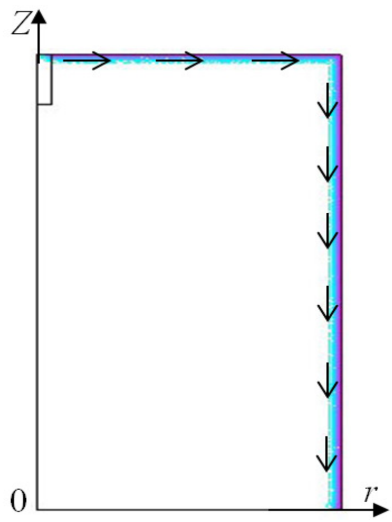

Fig. 3 – Distribution of current lines in the melt

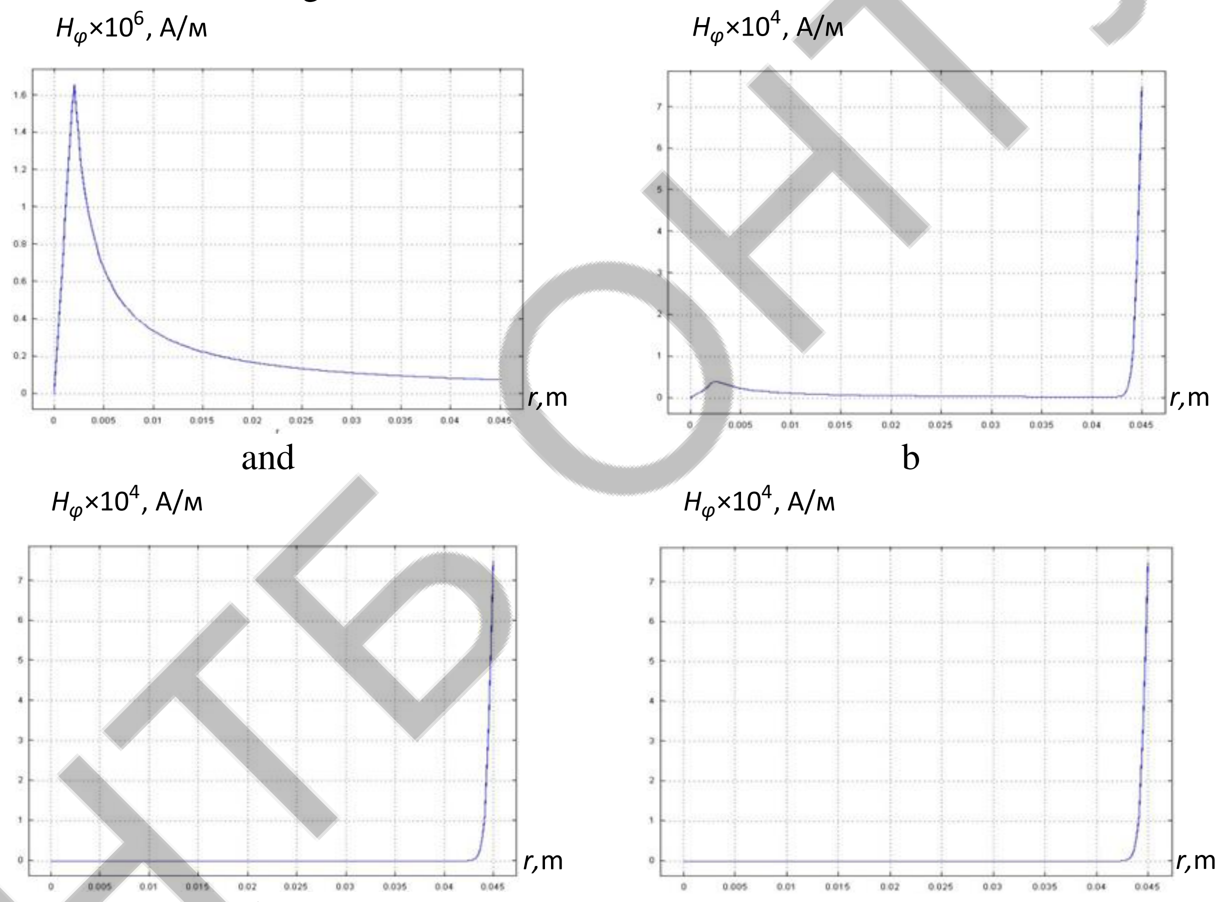

Fig. 4-Distribution of the magnetic field in different sections of the conductor at the maximum amplitude of the discharge current
a – melt mirror; b – Hк = 88·10-3 m; in – Hk = $45\cdot10^{-3}$m; d - the bottom of the bucket

We use the equation to find $P_{ем}$:

$$P_{ем} = \frac{\mu_r \mu_0 H^2}{2}, \qquad (16)$$

where $P_{ем}$ – magnetic pressure, Pa.

We will obtain distributions of the magnetic pressure amplitude(Fig. 5).

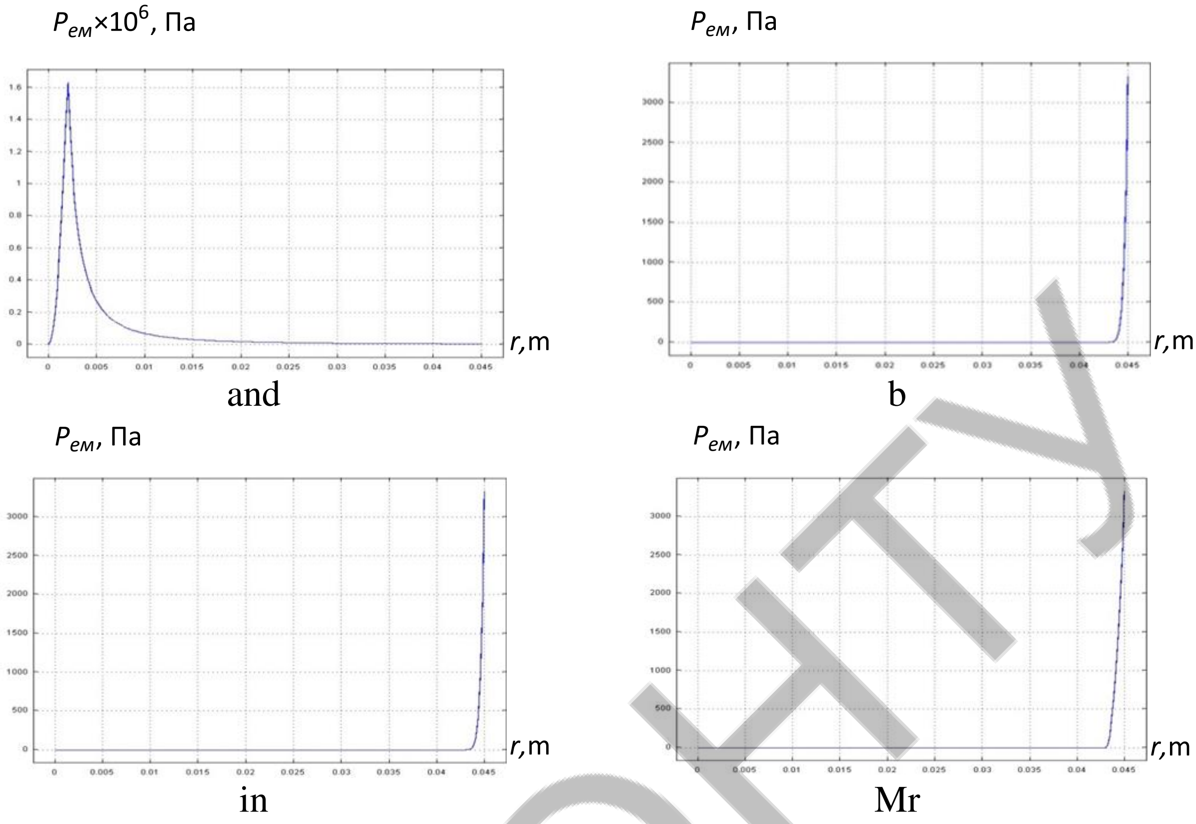

Fig. 5 – Distribution of magnetic pressure in different sections of the ladle at the maximum amplitude of the discharge current

2.2. Electrode system "Point - point"

This case describes a cylindrical ladle with a melt, through the mirror of which an electrode-current conductor is introduced [5]. The bucket itself is completely lined, but in the center of this part there is a round counter electrode, the diameter of which is equal to the diameter of the electrode-current conductor (Fig. 6).

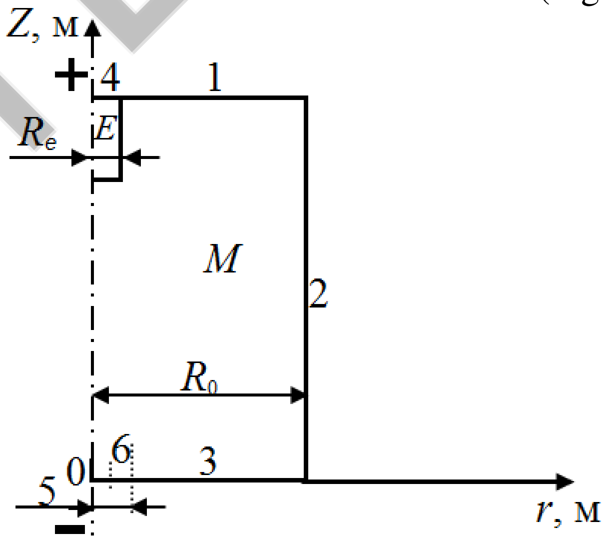

Fig. 6 – Geometry of the conductor for the electrode system "Point - point"

M– liquid cylindrical conductor (aluminum melt) with radius R0; *IS*– electrode with radius Re; 1 – melt mirror; 2 – side wall; 3 – ladle bottom; 4 – cross section of the electrode; 5 – counter electrode; 6 – skin layer thickness Δskin

The same module and equation are used as for the tip-plane electrode system. On the Z axis $H_\varphi = 0$. Initial conditions: $H_\varphi\big|_{t=0} = 0$ and $I\big|_{t=0} = 0$.

Boundary conditions:

For area 1: $$H_\varphi = \frac{I(t)}{2 \cdot \pi \cdot r}, \tag{17}$$

For area 2: $$H_\varphi = \frac{I(t)}{2 \cdot \pi \cdot R_0}, \tag{18}$$

For area 3: $$H_\varphi = \frac{I(t)}{2 \cdot \pi \cdot r}, \tag{19}$$

For area 4: $$H_\varphi = \frac{I(t) \cdot r}{2 \cdot \pi \cdot R_e^2}, \tag{20}$$

For area 5: $$H_\varphi = 0, \tag{21}$$

For area 6: $$H_\varphi = \frac{I(t) \cdot (r - R_0 + \Delta_{\text{скін}})}{2 \cdot \pi \cdot R_0 \cdot \Delta_{\text{скін}}}, \tag{22}$$

Current lines in this case will be distributed as shown in (Fig. 7).

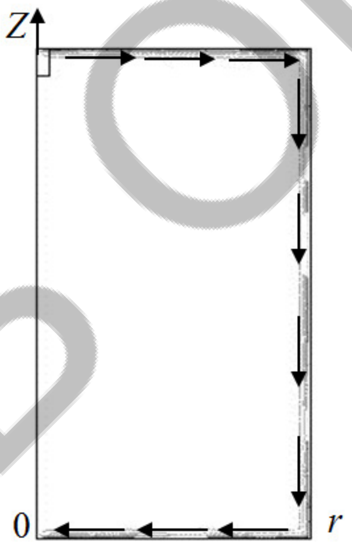

Fig. 7 - Distribution of current lines in the melt

The distribution of the magnetic field amplitude in different sections of the ladle at the maximum amplitude of the discharge current is shown in (Fig. 8), the distribution of the magnetic pressure in different sections of the ladle at the maximum amplitude of the discharge current is shown in (Fig. 9).

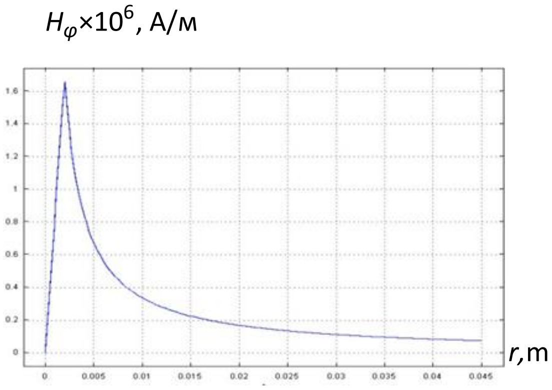

and

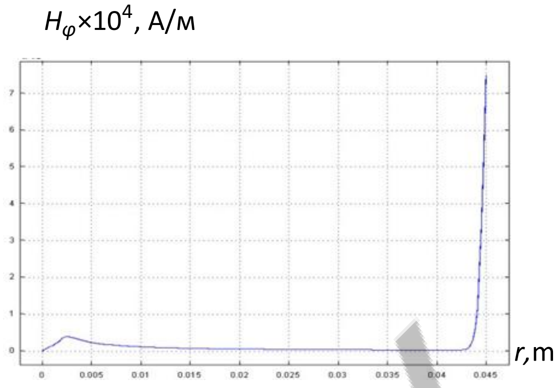

b

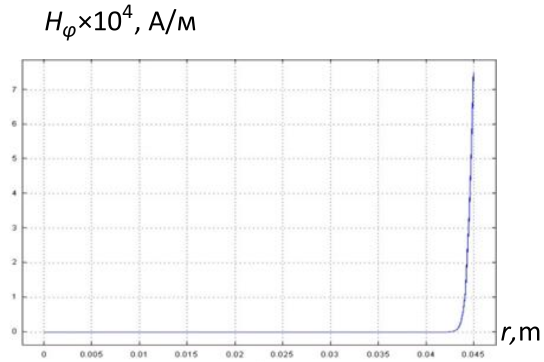

in

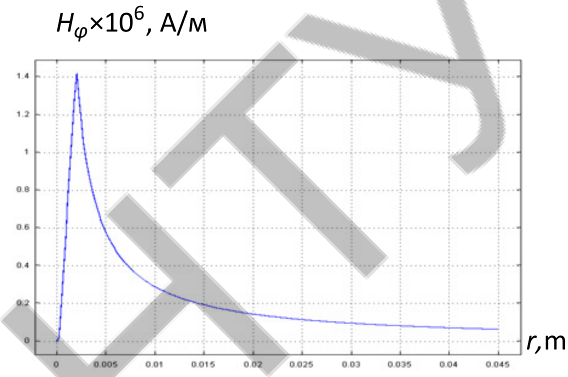

Mr

Fig. 8 – Distribution of the magnetic field in different sections of the ladle at the maximum amplitude of the discharge current
a – melt mirror; b – Hk = 88·10-3 m; c – Hk = 45·10-3 m; d - the bottom of the bucket

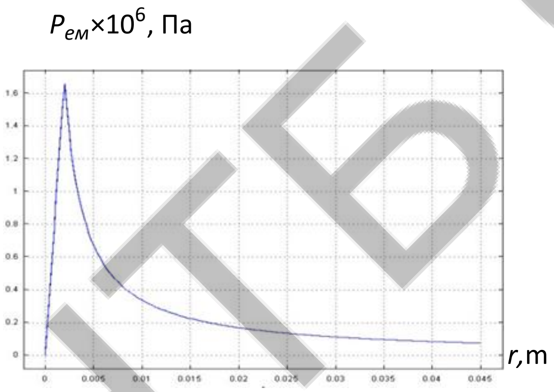

and

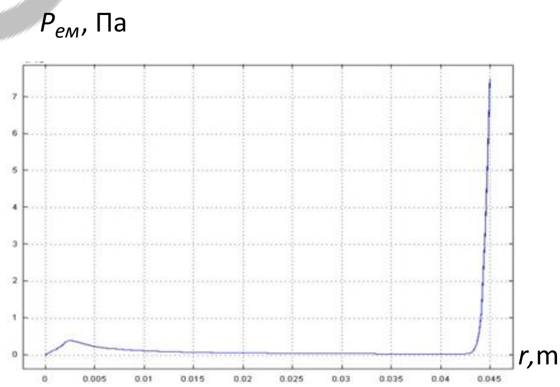

b

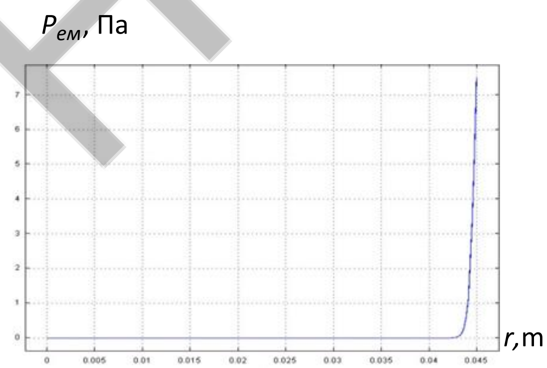

in

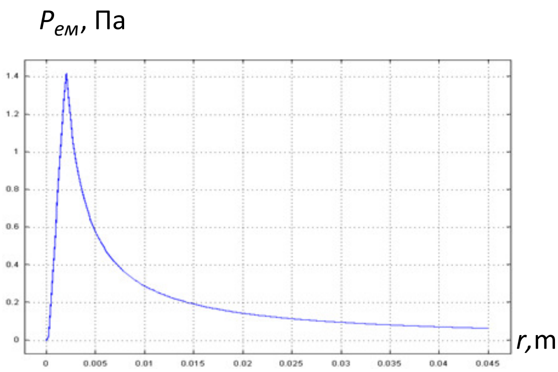

Mr

Fig. 9 – Distribution of magnetic pressure in different sections of the ladle at the maximum amplitude of the discharge current

2.3. Electrode system "Point - ladle walls"

The "Tip - walls of the ladle" electrode system consists of a current-carrying electrode immersed in the melt, a ladle with aluminum melt, in which the bottom is lined [6].

Estimates show that at a temperature of more than 650ºC, the values of electrical resistance (conductivity) of the material of the ladle walls and the melt are practically the same, so limit 2 is transparent to electromagnetic fields, and we do not take it into account.

The same module and equation as before are used. On the Z axis $H_\varphi = 0$. Initial conditions: $H_\varphi\big|_{t=0} = 0$ and $I\big|_{t=0} = 0$.

Boundary conditions:

For area 1: $$H_\varphi = \frac{I(t)}{2\cdot\pi\cdot r}, \tag{23}$$

For area 3: $$n \times E = 0, \tag{24}$$

For area 4: $$H_\varphi = \frac{I(t)\cdot r}{2\cdot\pi\cdot R_e^2}, \tag{25}$$

For area 5: $$H_\varphi = \frac{I(t)}{2\cdot\pi\cdot(R_0 + Ш)}, \tag{26}$$

For area 6: $$H_\varphi = \frac{I(t)\cdot(r-(R_0+Ш)+\Delta_{скін})}{2\cdot\pi\cdot(R_0+Ш)\cdot\Delta_{скін}}, \tag{27}$$

Expression (23) takes into account the so-called "magnetic isolation", i.e. at boundary 3 the normal component of the magnetic field is zero.

The following figures show how the electric current and magnetic field are pushed to the surface of the conductor (melt). This leads to the fact that the magnetic pressure in the bucket is distributed non-potentially (significantly unevenly). A significant concentration of the electromagnetic field and pressure in the near-electrode zones has also been established, which can be the cause of the excitation of eddy currents, the nature of which movement will be determined by the geometry of the electrode system and the nature of the deviation of electric current lines from a straight path (by the degree of scanning) (Fig. 10).

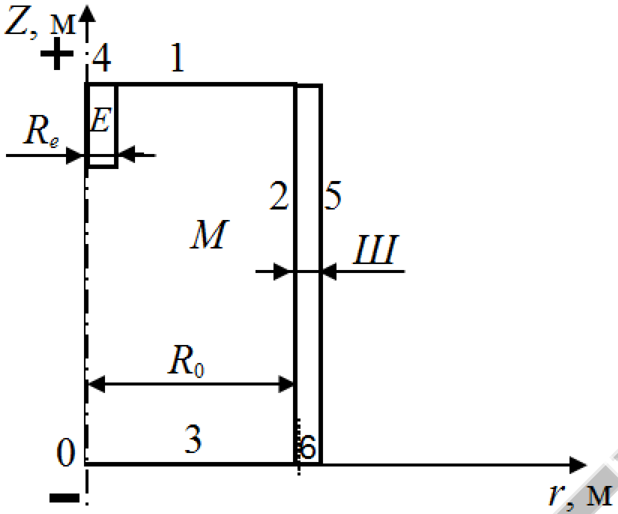

Fig. 10 - Geometry of the ladle with melt for the electrode system "Point - ladle walls" M – liquid cylindrical conductor (aluminum melt) with radius R0; E – electrode with a radius of Re; Ш – width of the wall of the ladle0.005 m;1 – melt mirror; 2 – side wall; 3 – bottom ladle; 4 – cross-section of the electrode; 5 – counter electrode; 6 – the thickness of the skin layer Δskin

In this case, the current will flow along the melt mirror and unlined steel walls, and the current lines (Fig. 11) in this case will be distributed. Since the main part of the current flows in the area of the melt mirror, we will limit ourselves to the distribution of the magnetic field and pressure only in this area (Fig. 12, see the appendix).

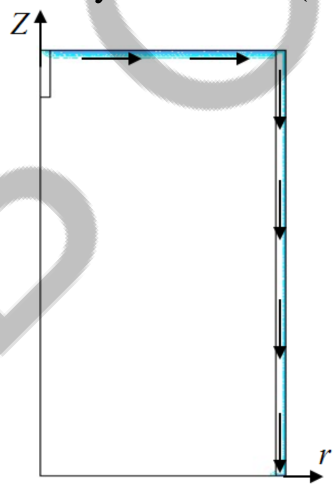

Fig. 11 – Distribution of current lines in the melt

The results of the calculations also showed that in the case of the "point - plane" and "point - point" electrode systems, at the maximum amplitude of the discharge current Imax = 22 kA, the pressure in the wall region of the melt does not exceed several kPa, which cannot significantly affect the state of the melt. In the case of the "Tip - ladle wall" electrode system, the electromagnetic field penetrates into the open steel wall of the ladle, there is a skin layer, and the magnetic pressure on the side surface of the melt is zero [7]. Meanwhile, the experimental application of such an electrode system made it possible to obtain positive changes in the structure and properties of the metal. This discrepancy can be explained by the fact that the calculations assumed conductivity for pure aluminum. For high-temperature aluminum melts (alloys), such reference data are not available, but obviously that the conductivity for alloys will be lower, and the ratio of the conductivity of the melt and the steel wall will change as it cools. Thus, the real distribution of the current when using the electrode system "Tip - ladle wall" at different moments of time could differ from that shown in (Fig. 11), which will definitely need to be taken into account when modeling physical processes in the solidifying (crystallizing) melt.

III. OBJECT, SUBJECT, AND METHODS OF RESEARCH

Relevance of work. Increasing the service life of rural-urban parts. machines is one of the main tasks facing the engineers of the agro-industrial complex. One of the ways to solve this problem is to develop new alloys and improve existing ones. There are many methods of improving the quality of cast metal. Functional capabilities of these methods are multifaceted and multipurpose. But there is no single universal method capable of affecting metal equally effectively. One of these new methods is the treatment of crystallizing liquid metal with an electric pulse discharge. Previous studies have shown that such processing has a sufficiently high efficiency. At the same time, it remains innovative and currently underexplored.

Therefore, to solve this problem, it is advisable to develop electrical equipment for the implementation of the technology of non-baking processing of metals and alloys.

The purpose of the work and research tasks: development of an electric discharge unit for non-furnace metal processing for the production of wear-resistant parts of agricultural machinery.

To achieve the specified goal, the following tasks must be solved in the work:

– conduct an analysis of existing electrode systems for high-voltage electric pulse treatment

– to carry out modeling of electric discharge processes of processing metals and alloys with high-voltage pulsed current at the crystallization stage.

– perform an experimental study of the influence of the parameters of the electric discharge installation on the crystallization process, structure and properties of aluminum alloys.

Object of study -processes that occur during electropulse processing of metals and design features of electrode systems for processing melts.

Subject of study–electric discharge processes that contribute to changing the structure of metals.

Research methods. Numerical and graphic methods are used in the work,methodsmathematical analysis, mathematical modeling and experimental research.

IV. RESULTS

The energy source for high-voltage electric pulse processing of the melt is the Pulse Current Generator (GIS), which is a battery of parallel-charged capacitors, the number, voltage and capacity of which determine its energy. Energy in the battery accumulates over a relatively long time interval and is released in a shorter time interval in the melt [8].

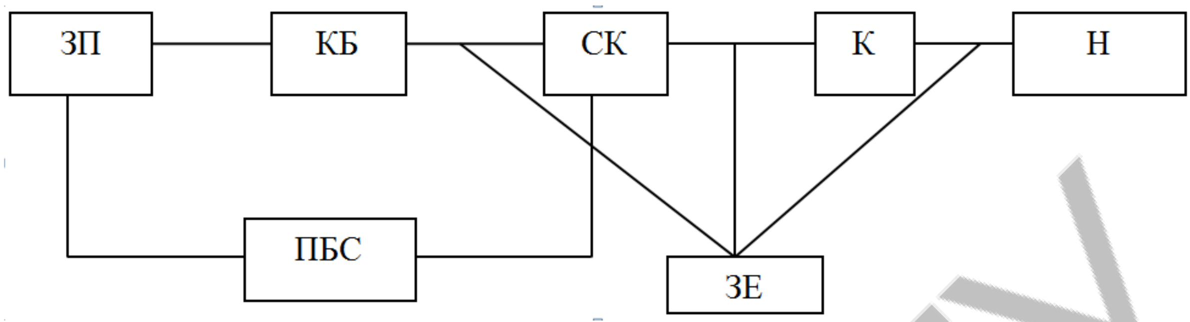

Fig. 13 – Structural diagram of GIS: ZP – charger; KB – capacitor battery; SC – switching system; K – collector; PBS - blocking and synchronization device; H – load; ZE - connecting elements

Calculations of the main GIS parameters were carried out according to the following formulas.

Energy stored in the capacitor bank W0:

$$W_0 = \frac{C \cdot U_0^{\,2}}{2}, \tag{28}$$

where C –capacitor battery capacity, F; U_0 –voltage to which the capacitors are charged, V.

Average power at the output of the generator P_{cp} is equal to:

$$P_{cp} = W_0 \cdot f, \tag{29}$$

where f – frequency of observing discharge pulses, Hz.

The average charging current of the capacitor bank I_{cp}:

$$I_{cp} = C \cdot U_0 \cdot f, \tag{30}$$

Power consumption of the charger P_{nom} is equal to:

$$P_{nom} = \frac{P_{cp}}{\eta}, \tag{31}$$

where η – coefficient of useful action of the charging circuit (in our case, we accept the value η from 0.7 to 0.8).

Based on the average charging current of the capacitor bank I_{cp} and power consumption P_{nom} a standard rectifier transformer is selected, on the basis of which the GIS is laid out.

In order to evaluate the electrical characteristics of the GIS during discharge, it is necessary to consider the transient process of discharge of the liquid metal capacity storage device [9]. Since the full calculation of transient processes in GIS is extremely cumbersome, let's limit ourselves to the simplified equivalent circuit of the discharge circuit presented in (Fig. 14), which allows us to calculate the necessary discharge characteristics of high-voltage equipment.

Since the capacitor battery will work on an inductive load in the oscillating discharge mode, since the melt is a medium with high conductivity, the dependence of the discharge current on time I(t) can be represented in the form of a decaying sinusoid:

$$I(t) = \frac{I'}{\sqrt{1-\gamma^2}} \cdot exp(-\gamma \cdot t) \cdot sin(\sqrt{1-\gamma^2} \cdot t), \quad (32)$$

$$I' = U_0 \cdot \sqrt{C/L}, \quad (33)$$

$$\gamma = 0{,}5 \cdot R \cdot \sqrt{C/L}, \quad (34)$$

where R is the active resistance of the discharge circuit, Ohm. R=Rdzh+Rp+Pрозп+Pпр – active resistance of the accumulator, discharger, fuse and connecting wires, Ohm;

L– the inductance of the discharge circuit, Hn. L=Lzh+Lp+Lрозп+Лпр – internal inductance of the accumulator, inductance of the discharger, own inductance of the melt and connecting wires.

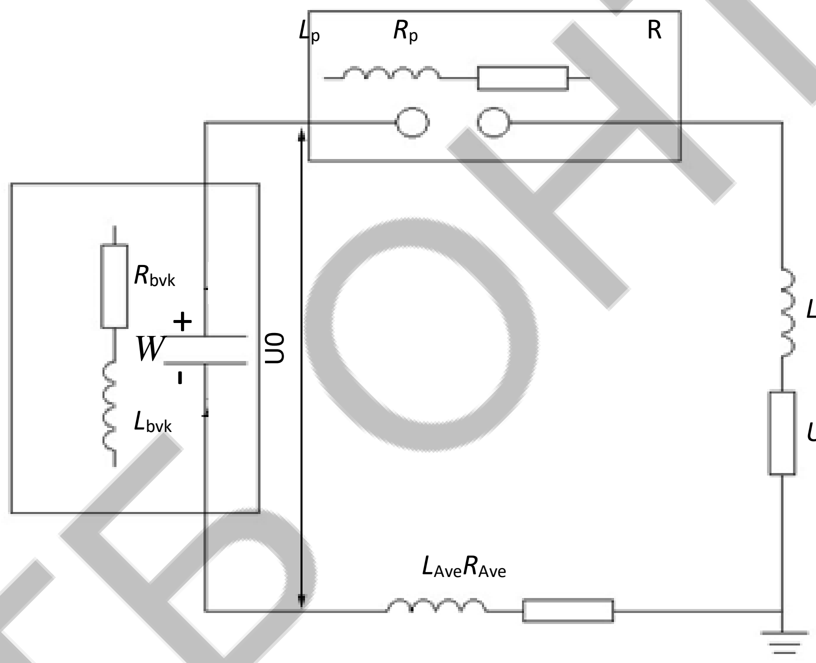

Fig. 14 - Equivalent circuit diagram of the GIS discharge circuit: BVK - battery of high-voltage capacitors; Lbvk – internal inductance of the storage device; Rbvk – active resistance of the accumulator; P - air spark arrester; Lp - inductance of the arrester; Rp – active resistance of the arrester; Lrozp – intrinsic inductance of the melt; Rrozp – melt resistance; Lpr - inductance of connecting wires; Rpr – active resistance of connecting wires.

The maximum possible current amplitude at discharge Imax:

$$I_{макс} = \frac{U_0}{\sqrt{\frac{L}{C}}}, \quad (35)$$

Maximum power $P_{макс}$, which develops in the load until the moment of maximum current is determined from the expression:

$$P_{\text{макс}} = 2 \cdot U_0 \cdot I' \cdot \gamma \cdot \exp\left(\frac{-2 \cdot \gamma}{\sqrt{1-\gamma^2}} \cdot \arcsin\sqrt{1-\gamma^2} \right), \qquad (36)$$

4.1. Results of aluminum processing of technical purity

With the use of aluminum of technical purity, a study was conducted on the possibility of suppressing transcrystallization (growth of columnar grains from the periphery to the center along the entire cross-section of the ingot or casting) due to the processing of the melt in the solid-liquid state. In this temperature range, the process of formation and growth of solid phase nuclei begins. The peculiarity of the formation of columnar structures is that the process of crystal nucleation begins on a more cooled surface, and the growth process proceeds in the opposite direction to the heat sink, that is, from the wall of the mold to the center of the ingot [10]. As already mentioned, pure aluminum itself is prone to transcrystallization. For a more stable realization of this phenomenon during the experiment, directed heat removal from the crystallizing melt was created artificially. First, the melt was poured into cold molds (without pre-heating to 450 ºC), secondly, the container with the melt was placed on a massive copper platform, which served as both a negative electrode and a refrigerator. The role of the second refrigerator was performed by the upper electrode placed in the melt (electrode system No. 1).

The idea of this study was that crystal nucleation begins in a thin near-surface layer of the melt, through which a pulse of discharge current flows through the skin effect. Due to Joule's release of heat in this layer, it was assumed to give the crystallization process a volumetric character due to the thermal interaction of the current with the crystals that have already formed and the reduction of the temperature gradient across the cross section of the ingot (thermostat model).

(Fig. 15) shows the cooling curve of aluminum near the bottom of the mold, from which it can be seen that the crystallization process proceeds quite quickly, and the region of the solid-liquid state takes from 50 to 55 seconds. Guided by these data, the treatment duration t was varied, with constant energy parameters of the VEO – C=1 μF; U0 = 7 kV; f = 2 Hz; W0 = 25 J; T = 9 μs; Imax = 5 A. The duration of VEO is presented in table 1, and the temperature interval is indicated by points on (Fig. 15, see the appendix).

The macrostructure of the obtained ingots is characterized by the presence of a well-defined lower zone of columnar crystals and a less pronounced upper zone. The central part of the samples is the equiaxed grain zone. VEO contributes to the narrowing of the lower columnar zone and the grinding of macrostructures, although it was not possible to completely suppress the directed grain growth.

Table 1

Duration of VEO at different temperature intervals

No. sample	1	2	3	4
τ, with	40	80	60	100
Temperature interval (Fig. 14)	AV	AC	DV	DS

The macrostructure improves as the processing interval increases, when the VEO starts slightly above the melting temperature and partially captures the solid state region. This is quite evident, since the crystallization process is non-equilibrium and the true state of the metal may not correspond to the temperature readings.

The analysis of experimental data shows that in order to completely prevent columnar crystallization, it is necessary to increase the power of action not only due to the current strength, but, first of all, due to the frequency of current pulses, comparing it with the linear growth rate of the interfacial surface. In other words, the frequency of the pulses should be such that each subsequent pulse "melts" the thin bases of the crystals that appear on the walls of the mold, preventing their fixation and growth.

Table 2

Indicators of the macrostructure of aluminum

No. sample	control	1	2	3	4
Height of the zone of columnar crystals, mm	35	30	22	21	22
Diameter of columnar grains, mm	5,6	4.7	4.3	3.7	3.7
Diameter of equiaxed grains in the center, mm	5.7	4.7	4.2	3.6 (dendrites)	2.7 (dendrites)

4.2. Results of AK7h alloy processing

AK7ch alloy was processed, using a high-voltage source GIS 12-18/0.25 and two electrode systems: electrode system No. 1 and No. 2. To determine the time to remove overheating of the melt and the temperature-time interval of processing, the cooling curves of the melt were recorded in advance. (Fig. A.1 Appendix A) presents thermograms taken in the center and near the wall of the mold, which allow us to see that the temperature gradient across the cross section of the crystallizing ingot is only a few degrees, that is, the melt crystallized as a single entity. Based on the cooling curve, a temperature of 6200C and duration were selected for the start of processing τ= 5 min., which corresponded to the crystallization interval of the primary a-phase. Conducting a preliminary thermographic analysis also made it possible to establish the chemical composition of the alloy: 6.71% Si; 0.14% Mg; <0.2% Mn; 0.11% Cu; 0.26% Zn; <0.1% Ni; < 0.1 Fe.

The VEO parameters given in Table 3 allow us to note the use of a small current passing through the melt and a slight decrease (up to0.7 mm) of the thickness of the skin layer.

Table 3

VEO parameters of AK7h alloy

Sample No	1	2	3	4
Capacity*WITH*, μF	0.25	0.25	0.25	0.25
High-voltageU_0, kV	12	12	12	12
The frequency of compliance with impulses*f*, Hz	1	6	1	6
Stored energyW_0, J	18	18	18	18
Discharge current period*T*, mks	5	5	5	5
The amplitude of the discharge current*Imax*, kA	4	4	4	4
No. electrode system	2		1	

The structure of ingots obtained as a result of VEO is dense, dendritic. The results of the metallographic analysis (table.4.) show that the VEO of the crystallizing melt, in contrast to processing in the quasi-two-phase region, has a positive effect on all structural components already at such a small energy in the pulse as W0 = 18 J (respectively, a small force current). The structure of the ingots is dense, dendritic throughout the cross-section. However, after VEO there is a tendency to the formation of a more dispersed and less oriented dendrite. After processing, particles of brittle eutectics are also crushed, needles of iron phases are transformed.

Table 4

Parameters of the microstructure of AK7ch alloy samples

Sample No	Size grains, μm	Eutectic volume, %	The length of the particles*Si*in the eutectic, μm	Iron phase
Control	170	19	108	needles 100 μm long
1	166	22	97	needles 60 microns long
2	133	21	87	inclusion of a compact form with a diameter of 36 μm
3	138	21	95	inclusion of a compact form with a diameter of 50 μm
4	133	20	76	inclusion of a compact form with a diameter of 85 μm

4.3. Results of AK7 alloy processing

AK7 alloy was treated using GIS and three different electrode systems as a high-voltage source (table. 5). In addition, the current strength and the frequency of observing pulses varied. Based on the cooling curves (Fig. 16), a temperature of 620 0C was assumed for the beginning of processing, as well as for the AK7h alloy, and the duration was τ= 5 min. The use of laboratory GIS made it possible to study the influence of higher energy regimes of VEO on the structure and properties of the alloy. Conducting a chemical analysis of the alloy (7.0% Si; 0.23% Mg; 0.22% Mn; 1.45% Cu; 0.34% Zn; 0.04% Ni; 0.68% Fe) made it possible to determine several higher iron content and increased copper content. On the one hand, the composition of these elements meets the requirements of DSTU 2839-94, on the other hand, the higher iron content made it possible to study in more detail the effect of VEO on harmful ferrous phases.

Table 5

VEO parameters of AK7 alloy

Sample No	Processing parameters					
	WITH, μF	U_0, kV	*f*, Hz	W_0, J	*T*, mks	*Imax*, kA
Electrode system No. 1						
control	–	–	–	–	–	–
1	1	7	2	25	9	5
2	1	7	6	25	9	5
3	1	20	2	220	9	16
Electrode system No. 2						
control	–	–	–	–	–	–
4	1	7	2	25	9	5
5	1	7	6	25	9	5
6	1	20	2	220	9	16
Electrode system No. 3						
control	–	–	–	–	–	–
7	1	7	2	25	9	5
8	1	7	6	25	9	5
9	1	20	2	220	9	16

Diagrams are presented in (Fig. 17, see the appendix) that allow analyzing the influence of processing parameters and electrode systems on the granular structure. It can be seen that the control ingots contain a large, almost equiaxed grain along the entire section. Increasing the power of the current action on the crystallizing metal, in comparison with the VEO of the AK7h alloy, where the degree of grain grinding was 1.3 times, led to grinding of the grain structure from 1.5 to 3 times. Moreover, the most effective in this regard is electrode system No. 2 - two electrodes immersed in the melt. It should also be noted that, despite the fact that the depth of immersion of the electrodes was all5 mm, changes in the structure are observed over the entire cross-section of the ingot. With an increase in the power of action, the extent of changes in the structure increases. However, it is not possible to separate the contribution of the frequency of pulses and the current strength at this stage, since samples No. 4 and No. 5 correspond to the same power and, as we can see, the degree of change in the structure is the same.

V.CONCLUSIONS

1. The analysis of existing scientific works, patents and literature in the field of non-bake metal processing allows us to single out several main areas, among which the least researched and promising is pulse-periodic current processing.

2. The electrical characteristics of the discharge current pulse in two phase states were studied: liquid and liquid-solid. The frequency range (from 85 to 115 kHz) in which the maximum of the spectral density is concentrated is revealed. It was found that as the temperature of the melt decreases, the maximum of the spectral density shifts to lower frequencies and the reactive component of the resistance changes.

3. High-voltage electropulse processing of the melt in the crystallization interval, compared to processing in the liquid state, has a significant effect on the structure of aluminum of technical purity, which hardens under the conditions of directional heat removal. With VEO using Imax = 5 kA and $f = 2$ Hzachieved reduction of the zone of columnar crystals by 1.5 times and grinding of equiaxed dendrites by 2 times. During VEO of the hardening metal, there is a steady dependence of the parameters of the structure and properties on the power of action: with an increase in the power of action on the hardening Ak7ch and AK7 alloys, the granular structure is crushed, the degree of dendrite disorientation and the degree of compaction of brittle components increases, and plasticity increases.

The scheme of processing with two submerged electrodes is preferred for VEO of a hardening metal.

The proposed mechanism of high-voltage electropulse processing, effective in the processing of crystallizing metal, with which the main contribution to the change in the state of the melt, structure and properties of the metal can be attributed, namely, the effect of VEO on the rate of formation of crystallization centers, and the electrotechnical equipment for the implementation of this mechanism has been developed.

VI.REFERENCES

1. Electrotechnical complex for discharge-pulse synthesis of carbon nanomaterials with different magnetic properties / L. Z. Boguslavskyi, N. S. Nazarova, L. E. Ovchinnikova, D. V. Vynnychenko, V. V. Dyordiychuk // Techn. electrodynamics. - 2012. - No. 3. - P. 107-108.

2. Investigation of the processes of the interaction of a powerful electric discharge current pulse with a liquid metallic medium: research report (interim): No. IV-11-07/ IIPT of the National Academy of Sciences of Ukraine; hands V.N. Tsurkin; executed by: A.V. Synchuk - Nikolaev, 2007.- 39 p.- No. GR 0107U004479.- Inv. No. 993 – NS.

3. Yakukhin V. G. High-tech processing methods: textbook / Ed. Dr. Tech. Sciences, Prof. O. V. Taratynova. - Moscow: Moscow State University, 2011. - 362 p.

4. Bashmakova, N.V. Investigation of the effect of electric current on the crystallization and properties of aluminum alloys with an increased iron content: autoref. thesis to apply for a candidate's degree. technical Sciences: specialist 02.16.04 "Foundry production"/N.V. Bashmakov. – Novokuznetsk, 2007. – 16 p.

5. Dorofeev, A.V. Processing of aluminum melts with electric current / A.V. Dorofeev, A.B. Kylin, A.S. Tortyshnikov // Foundry of Russia. – 2002. – No. 2. – p. 19 – 21.

6. Deev, V.B. Influence of electric current on the crystallization of aluminum alloys containing iron / V.B. Deev, I.F. Selyanin, N.V. Bashmakova // Foundry of Russia. – 2007. - No. 8. – P. 12-15.

7. XiliangLiaoa. The refining mechanism of the electric current pulse on the solidification structure of pure aluminum / Xiliang Liaoa, Jun Luoa, Wenjie Chena, Yongyong Gong // School of Materials Science and Engineering.–2006.─№ 4.─P. 32─35.

8. Electrotechnical complex of current protection in high-voltage generators of impulse currents / D. V. Vinnychenko, N. S. Nazarova, I. L. Vinnychenko, Yu. O. Adamchuk // Nauk. Donets Ave. national technical university Ser. Electrical engineering and energy. – 2013. – Issue 2. - P. 54-58.

9. Chunyan Ban. Influence of pulse electric current on solidification structure of Al-Si alloy / Chunyan Ban, Yi Han, Qixian Ba, Jianzhong Cui //Electromagnetic Processing of Material. ─ 2007.─ No. 1.─P. 34-37.

10. Zarembo, V.I. The influence of current pulses on the processes of melting and crystallization of metals / V.I. Zarembo [and others] // Metallurgy of machine construction. - 2003. - No. 1. - P. 11-15.

APPENDICES

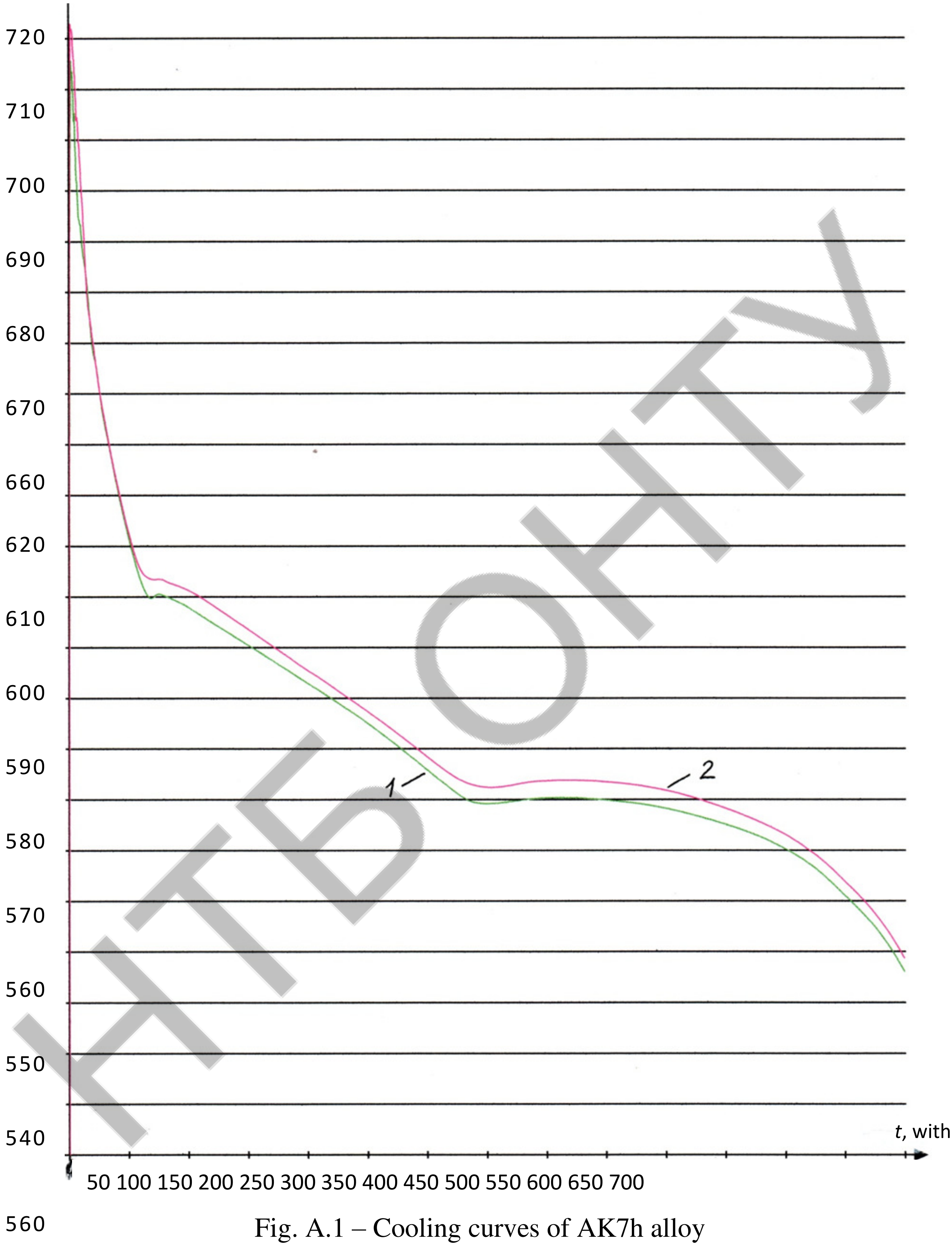

Fig. A.1 – Cooling curves of AK7h alloy
1– near the wall of the form; 2– in the center

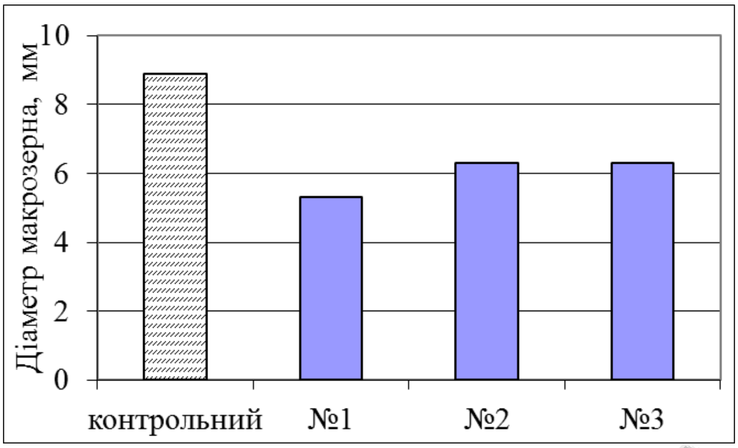

and

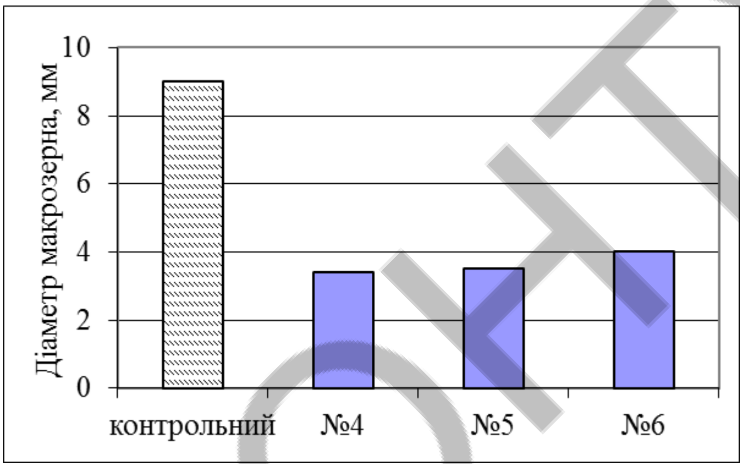

b

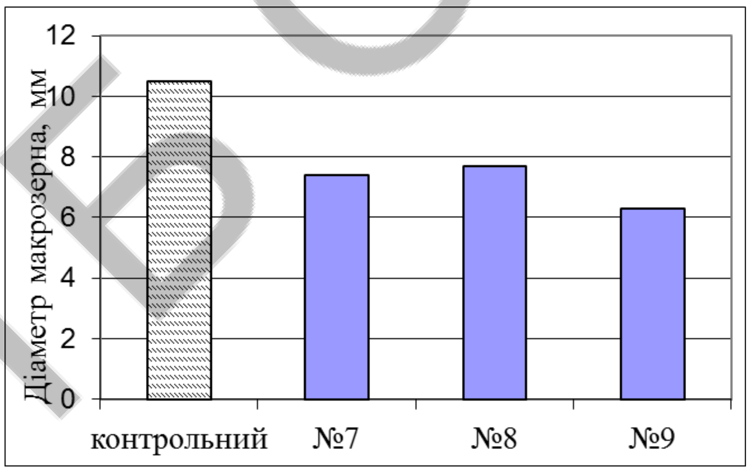

in

Fig. 17 – Influence of VEO on the macrostructure of the AK7 alloy: a, b, c - electrode systems No. 1; number 2; No. 3 respectively

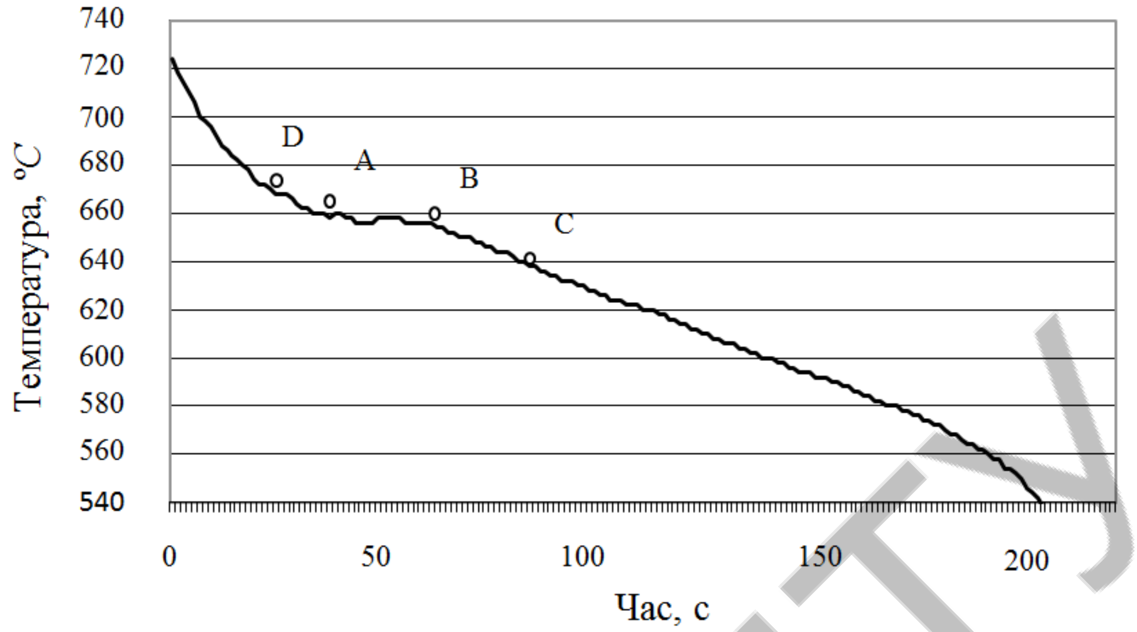

Fig. 15– Aluminum cooling curve near the bottom of the mold (near the copper cooler)

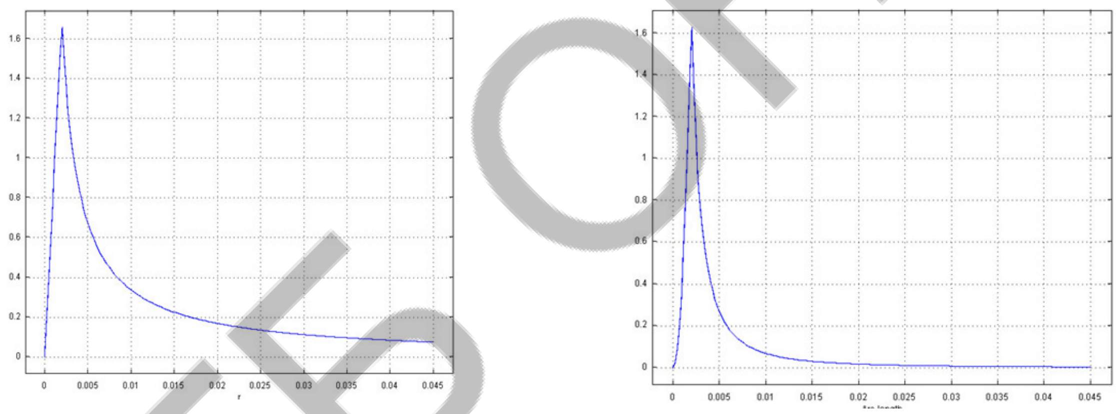

and b

Fig. 12 – Distribution of the magnetic field and pressure along the melt mirror
a – distribution of the magnetic field along the melt mirror; b – magnetic pressure distribution along the melt mirror